Deep Unfolded Hybrid Beamforming in Reconfigurable Intelligent Surface Aided mmWave MIMO-OFDM Systems

Kuan-Ming Chen, Hsin-Yuan Chang, Ronald Y. Chang, *Senior Member, IEEE*, and Wei-Ho Chung

***Abstract*—This letter considers a millimeter-wave (mmWave) multiple-input multiple-output (MIMO) orthogonal frequency division multiplexing (OFDM) transceiver system assisted by a reconfigurable intelligent surface (RIS). The goal is to jointly design transceiver hybrid beamforming and RIS phase shifts to maximize spectral efficiency (SE). We adapt the weighted minimum mean square error manifold optimization (WMMSE-MO) algorithm to the RIS-assisted system, and further deep-unfold it with neural networks to alleviate the algorithm's computational complexity and expedite its convergence. The proposed deep-unfolded WMMSE-MO algorithm demonstrates superior SE performance, convergence speed, and computational efficiency compared to both its counterpart without deep unfolding and previous methods.**

***Index Terms*—mmWave communication, MIMO-OFDM, reconfigurable intelligent surface, hybrid beamforming, deep unfolding.**

I. Introduction

MILLIMETER-WAVE (mmWave) communication offers high data rates and low latency but faces increased free-space path loss. Beamforming is essential to combat path loss. Hybrid beamforming with a partially-connected structure [1], which connects each radio frequency (RF) chain to a disjoint subset of antennas, is a cost-effective solution that reduces hardware costs, although it can lead to signal degradation when encountering obstacles due to beamforming's high directionality. Reconfigurable intelligent surfaces (RISs) address this issue by adjusting the phase shifts of reflecting elements to reflect signals, offering benefits such as interference mitigation, extended signal coverage, improved spectral and energy efficiency, and enhanced security [2], [3]. Therefore, RIS technology is crucial for enhancing capacity and channel conditions in future mmWave communication.

Existing joint RIS and mmWave transceiver designs aim to maximize spectral efficiency (SE), reduce bit error rates (BER), and optimize RIS functions [4], [5], [6]. In [4], the sparse nature of the mmWave channel was exploited to jointly design hybrid beamforming and RIS to maximize SE. In [5], a geometric mean decomposition (GMD) and principal component analysis (PCA) based approach was proposed for designing RIS and transceivers, which reduces BER. In [6], majorization-minimization (MM) and manifold optimization (MO) algorithms were compared for solving the RIS optimization problem, showing the advantages of MO. These optimization-based algorithms however require multiple iterations, leading to increased computation times.

To address this challenge, deep learning (DL) has emerged as a viable solution. DL-based methods have been employed in optimizing RIS-aided transmission [7], [8], [9]. In [7], a convolutional neural network (CNN) was used to predict RIS phase shifts and SE based on user locations. In [8], an unsupervised learning approach was used to design RIS with reduced complexity. In [9], a two-stage neural network based on unsupervised learning was employed for separate RIS and beamforming design in each stage. However, end-to-end DL models can face computational and memory challenges due to the growing number of trainable parameters. To address this, the deep unfolding technique [10], a model-driven DL approach, employs a compact set of trainable parameters by unfolding iterative algorithms into multi-layered neural networks. This technique has demonstrated its effectiveness in fully-digital beamforming design [11] and channel estimation [12] in RIS-aided systems, resulting in reduced complexity and enhanced performance. However, the challenge of jointly designing hybrid beamforming in RIS-aided mmWave MIMO-OFDM systems remains unexplored by the aforementioned algorithms.

In this letter, we address the joint design of partially-connected hybrid beamforming in RIS-aided mmWave MIMO-OFDM systems to maximize SE. We introduce a sequential optimization framework based on the weighted minimum mean square error MO (WMMSE-MO) algorithm for hybrid beamforming and RIS design, and we employ deep unfolding to expedite algorithm convergence by substituting the Armijo backtracking line search with a neural network in the WMMSE-MO algorithm. Our main contributions are:

- To the best of our knowledge, this letter presents the first exploration of the WMMSE-MO algorithm and its deep unfolding in RIS-aided mmWave MIMO-OFDM systems. The integration of deep unfolding into hybrid beamforming addresses the challenges such as complexity posed by iterative MO algorithms in RIS-aided systems.
- Simulation results show that deep unfolding achieves a remarkable computation time reduction while maintaining superior SE performance. Additionally, our method outperforms matrix factorization-based as well as GMD and PCA-based methods.

Notation: $|\cdot|$ and $\lfloor\cdot\rfloor$ are the absolute and floor operators, respectively. $\mathrm{diag}(\mathbf{x})$ and $\mathrm{Blkdiag}(\mathbf{x}_1, \mathbf{x}_2, \ldots)$ denote diagonal

Manuscript received 25 January 2024; accepted 1 February 2024. Date of publication 5 February 2024; date of current version 11 April 2024. This work was supported in part by the National Science and Technology Council, Taiwan, under Grant 112-2221-E-001-004-MY3 and Grant 110-2221-E-007-042-MY3. The associate editor coordinating the review of this article and approving it for publication was N. Saeed. *(Corresponding authors: Ronald Y. Chang; Wei-Ho Chung.)*

Kuan-Ming Chen and Hsin-Yuan Chang are with the Department of Electrical Engineering, National Tsing Hua University, Hsinchu 300, Taiwan (e-mail: kming.chen@m110.nthu.edu.tw; hyuan.chang@outlook.com).

Ronald Y. Chang is with the Research Center for Information Technology Innovation, Academia Sinica, Taipei 115, Taiwan (e-mail: rchang@citi.sinica.edu.tw).

Wei-Ho Chung is with the Department of Electrical Engineering, National Tsing Hua University, Hsinchu 300, Taiwan, and also with the Research Center for Information Technology Innovation, Academia Sinica, Taipei 115, Taiwan (e-mail: whchung@ee.nthu.edu.tw).

Digital Object Identifier 10.1109/LWC.2024.3362399

matrix with $\mathbf{x}$ on the diagonal and block diagonal matrix with $\mathbf{x}_i$'s on the diagonal, respectively. $(\cdot)^T$, $(\cdot)^H$, and $(\cdot)^{-1}$ denote transpose, conjugate transpose, and inverse operators, respectively. $\mathrm{tr}(\cdot)$, $\|\cdot\|_F$, $\|\cdot\|$, and $\det(\cdot)$ denote the trace, Frobenius norm, l_2-norm, and determinant of a matrix, respectively. $\mathbb{E}[\cdot]$ is the mathematical expectation. $\odot$ denotes the Hadamard product.

II. System Model and Problem Formulation

We consider a RIS-assisted single-user downlink mmWave MIMO-OFDM system. The direct path between the base station (BS), equipped with N_t antennas, and user equipment (UE), equipped with N_r antennas, is blocked by obstructions. The BS transmits the data streams $[\mathbf{x}_1,\ldots,\mathbf{x}_k,\ldots,\mathbf{x}_K] \in \mathbb{C}^{N_s\times K}$ to the UE through the RIS, where K is the number of subcarriers and N_s is the number of data streams, with $\mathbb{E}[\mathbf{x}_k\mathbf{x}_k^H]=\mathbf{I}_{N_s},\forall k$. Partially-connected hybrid beamforming is employed at the BS, with a baseband precoder $\mathbf{F}_{\mathrm{BB},k} \in \mathbb{C}^{N_t^{\mathrm{RF}}\times N_s}$ and an analog precoder $\mathbf{F}_{\mathrm{RF}}=\mathrm{Blkdiag}(\mathbf{f}_1,\mathbf{f}_2,\ldots,\mathbf{f}_{N_t^{\mathrm{RF}}}) \in \mathbb{C}^{N_t\times N_t^{\mathrm{RF}}}$, where $\mathbf{f}_m \in \mathbb{C}^{\lfloor\frac{N_t}{N_t^{\mathrm{RF}}}\rfloor\times 1}$ for $m=1,\ldots,N_t^{\mathrm{RF}}$ and N_t^{RF} is the number of RF chains at the BS. At the receiving end, by employing an analog combiner $\mathbf{W}_{\mathrm{RF}}=\mathrm{Blkdiag}(\mathbf{w}_1,\mathbf{w}_2,\ldots,\mathbf{w}_{N_r^{\mathrm{RF}}}) \in \mathbb{C}^{N_r\times N_r^{\mathrm{RF}}}$ followed by a baseband combiner $\mathbf{W}_{\mathrm{BB},k} \in \mathbb{C}^{N_r^{\mathrm{RF}}\times N_s}$, where $\mathbf{w}_m \in \mathbb{C}^{\lfloor\frac{N_r}{N_r^{\mathrm{RF}}}\rfloor\times 1}$ for $m=1,\ldots,N_r^{\mathrm{RF}}$ and N_r^{RF} is the number of RF chains at the UE, the decoded signal for the kth subcarrier is expressed as

$$\mathbf{y}_k=\mathbf{W}_k^H\mathbf{H}_{\mathrm{eff},k}\mathbf{F}_k\mathbf{x}_k+\mathbf{W}_k^H\mathbf{n}_k, \tag{1}$$

where $\mathbf{F}_k=\mathbf{F}_{\mathrm{RF}}\mathbf{F}_{\mathrm{BB},k} \in \mathbb{C}^{N_t\times N_s}$ and $\mathbf{W}_k=\mathbf{W}_{\mathrm{RF}}\mathbf{W}_{\mathrm{BB},k} \in \mathbb{C}^{N_r\times N_s}$, $\mathbf{H}_{\mathrm{eff},k}$ is the RIS-assisted effective channel at the kth subcarrier, and $\mathbf{n}_k \sim \mathcal{CN}(0,\sigma^2\mathbf{I}_{N_s})$ is the additive white Gaussian noise with σ^2 being the noise power. The effective channel $\mathbf{H}_{\mathrm{eff},k}$ can be expressed as $\mathbf{H}_{2,k}\mathbf{\Phi}\mathbf{H}_{1,k}$, where $\mathbf{H}_{1,k} \in \mathbb{C}^{M\times N_t}$ and $\mathbf{H}_{2,k} \in \mathbb{C}^{N_r\times M}$ are the BS–RIS channel and RIS–UE channel for the kth subcarrier, respectively, and $\mathbf{\Phi}=\mathrm{diag}(\phi_1,\ldots,\phi_M) \in \mathbb{C}^{M\times M}$ represents configurations of the M RIS elements, with $\phi_q=e^{j\widehat{\phi}_q}$ and $\widehat{\phi}_q \in [0,2\pi)$ for $q=1,\ldots,M$.

The frequency-domain channels $\mathbf{H}_{1,k}$ and $\mathbf{H}_{2,k}$ can be expressed through their corresponding delay-domain channels $\widetilde{\mathbf{H}}_{1,d}$ and $\widetilde{\mathbf{H}}_{2,d}$ as

$$\mathbf{H}_{i,k}=\sum_{d=0}^{D-1}\widetilde{\mathbf{H}}_{i,d}e^{-j\frac{2\pi k}{K}d},\ i=1,2, \tag{2}$$

where D is the length of the cyclic prefix. The dth delay tap of $\widetilde{\mathbf{H}}_{1,d}$ and $\widetilde{\mathbf{H}}_{2,d}$ comprises a line-of-sight (LoS) path and L non-line-of-sight (NLoS) paths [5], as described by

$$\widetilde{\mathbf{H}}_{1,d}=\sqrt{\frac{N_tM}{L+1}}\sum_{l=0}^{L}\kappa_l p(dT_s-\tau_l)\mathbf{a}_{\mathrm{RIS}}(\gamma_l^r,\eta_l^r)\mathbf{a}_{\mathrm{BS}}(\theta_l^t)^H, \tag{3}$$

$$\widetilde{\mathbf{H}}_{2,d}=\sqrt{\frac{N_rM}{L+1}}\sum_{l=0}^{L}\upsilon_l p(dT_s-\tau_l')\mathbf{a}_{\mathrm{UE}}(\theta_l^r)\mathbf{a}_{\mathrm{RIS}}(\gamma_l^t,\eta_l^t)^H, \tag{4}$$

where $p(\tau)$ is the rectangular pulse shaping filter for T_s-spaced signaling; τ_l and τ_l' (with $\tau_0=\tau_0'=0$) denote the relative time delay of the lth path; κ_l and υ_l are complex channel gains, with κ_0 and υ_0 of LoS component modeled by $\mathcal{CN}(0,1)$ and $\{\kappa_l\}_{l=1}^L$ and $\{\upsilon_l\}_{l=1}^L$ of NLoS components modeled by $\mathcal{CN}(0,10^{-0.1\mu})$ with a Rician factor μ; θ_l^t and θ_l^r denote the angles of departure (AoD) at the BS and angles of arrival (AoA) at the UE for the lth path, respectively; γ_l^t (γ_l^r) and η_l^t (η_l^r) are the azimuth and elevation AoD (AoA) at the RIS, respectively; and $\mathbf{a}_{\mathrm{BS}}$, $\mathbf{a}_{\mathrm{RIS}}$, and $\mathbf{a}_{\mathrm{UE}}$ are the steering vectors at the BS, RIS, and UE, respectively. Considering the uniform linear array (ULA) structure at the BS and UE, and the uniform planar array (UPA) structure at the RIS, the steering vectors are expressed as

$$\mathbf{a}_{\mathrm{BS}}(\theta)=\mathbf{a}_{\mathrm{UE}}(\theta)=\frac{1}{\sqrt{N}}\Big[1,e^{j\frac{2\pi d_a}{\lambda}\sin(\theta)},\ldots,e^{j\frac{2\pi d_a}{\lambda}(N-1)\sin(\theta)}\Big]^T, \tag{5}$$

$$\mathbf{a}_{\mathrm{RIS}}(\gamma,\eta)=\frac{1}{\sqrt{M}}\Big[1,\ldots,e^{j\frac{2\pi d_a}{\lambda}(m_y\sin(\gamma)\cos(\eta)+m_z\sin(\eta))},\ldots,e^{j\frac{2\pi d_a}{\lambda}((M_y-1)\sin(\gamma)\cos(\eta)+(M_z-1)\sin(\eta))}\Big]^T, \tag{6}$$

where d_a is the antenna spacing which is set to half wavelength $\frac{\lambda}{2}$, N represents N_t and N_r for the case of BS and UE, respectively, and M_y and M_z represent the numbers of horizontal and vertical elements of the RIS and $M=M_y\times M_z$.

Our objective is to optimize the average SE of the system through the design of hybrid beamforming and RIS beamforming. The SE at the kth subcarrier is given by

$$R_k=\log_2\det\Big(\mathbf{I}_{N_s}+\frac{1}{\sigma^2}\mathbf{W}_k^\dagger\mathbf{H}_{\mathrm{eff},k}\mathbf{F}_k\mathbf{F}_k^H\mathbf{H}_{\mathrm{eff},k}^H\mathbf{W}_k\Big), \tag{7}$$

where $\mathbf{W}_k^\dagger=(\mathbf{W}_k^H\mathbf{W}_k)^{-1}\mathbf{W}_k^H$. Then, the problem is formulated as

$$\max_{\mathbf{F}_{\mathrm{RF}},\mathbf{F}_{\mathrm{BB},k},\mathbf{\Phi},\mathbf{W}_{\mathrm{RF}},\mathbf{W}_{\mathrm{BB},k}}\ \frac{1}{K}\sum_{k=1}^{K}R_k \tag{8a}$$

$$\text{s.t.}\quad \|\mathbf{F}_k\|_F^2\le N_s,\forall k, \tag{8b}$$

$$|\mathbf{f}_m(n)|=1,\forall m,n, \tag{8c}$$

$$|\mathbf{w}_m(n)|=1,\forall m,n, \tag{8d}$$

$$|\phi_q|=1,\forall q=1,2,\ldots,M, \tag{8e}$$

where $\mathbf{f}_m(n)$ ($\mathbf{w}_m(n)$) is the nth element in $\mathbf{f}_m$ ($\mathbf{w}_m$) with $\lfloor\frac{N_t}{N_t^{\mathrm{RF}}}\rfloor$ ($\lfloor\frac{N_r}{N_r^{\mathrm{RF}}}\rfloor$) elements [13]. Problem (8) is nonconvex due to the transmit power constraint (8b) and constant modulus constraints (8c)–(8e). To tackle this challenging problem, we consider manifold optimization (MO)-based algorithms used in hybrid beamforming scenarios, both with RIS [14] and without RIS [13]. We address the inherent high complexity resulting from the iterative nature of the MO algorithm by applying deep unfolding. Deep unfolding is especially valuable in scenarios involving RIS, as the complexity of the iterative algorithm increases with the presence of RIS.

III. Deep-Unfolded Joint Hybrid Beamforming and RIS Optimization

The original problem (8) is transformed into an equivalent weighted minimum mean square error (WMMSE) problem, as

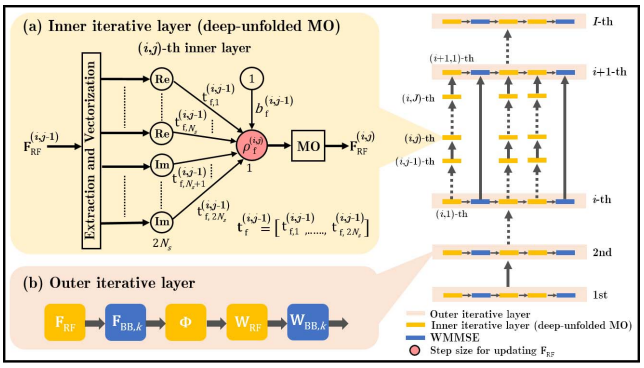

Fig. 1. The deep-unfolded WMMSE-MO algorithm.

expressed in problem (9), through manipulations that include the derivation of optimal weight matrices and substitution of variables, ensuring identical global optimal solutions [13]:

$$\min_{\substack{\mathbf{F}_{\mathrm{RF}},\mathbf{F}_{\mathrm{BB},k},\boldsymbol{\Phi},\mathbf{W}_{\mathrm{RF}},\mathbf{W}_{\mathrm{BB},k},\\ \xi_k,\boldsymbol{\Lambda}_k}} \quad \frac{1}{K}\sum_{k=1}^{K}\mathrm{tr}\big((\boldsymbol{\Lambda}_k\mathbf{E}_k)-\log_2\det(\boldsymbol{\Lambda}_k)\big) \tag{9a}$$

$$\text{s.t.} \qquad (8b),\ (8c),\ (8d),\ (8e), \tag{9b}$$

where $\boldsymbol{\Lambda}_k$ and $\mathbf{E}_k$ represent a weight matrix and modified mean MSE for the kth subcarrier, respectively, and ξ_k denotes the scaling factor. The modified MSE is given by [13]

$$\begin{aligned}\mathbf{E}_k &= \mathbb{E}\big[\big\|\mathbf{x}_k-\xi_k^{-1}\mathbf{y}_k\big\|^2\big]\\ &= \big(\mathbf{I}_{N_s}-\xi_k^{-1}\mathbf{W}_k^H\mathbf{H}_{\mathrm{eff},k}\mathbf{F}_k\big)\big(\mathbf{I}_{N_s}-\xi_k^{-1}\mathbf{W}_k^H\mathbf{H}_{\mathrm{eff},k}\mathbf{F}_k\big)^H\\ &\quad+\xi_k^{-2}\sigma^2\mathbf{W}_k^H\mathbf{W}_k.\end{aligned} \tag{10}$$

We propose a novel algorithm based on the WMMSE-MO algorithm originally designed for scenarios without RIS considerations [13] to solve problem (9). Our proposed algorithm adopts a nested iterations framework that incorporates both inner and outer iterations, as illustrated in Fig. 1. The I stacked rectangles represent I outer layers, and within each outer iteration i, the algorithm updates $\mathbf{F}_{\mathrm{RF}}^{(i)}, \mathbf{F}_{\mathrm{BB},k}^{(i)}, \boldsymbol{\Phi}^{(i)}, \mathbf{W}_{\mathrm{RF}}^{(i)}, \mathbf{W}_{\mathrm{BB},k}^{(i)}$ sequentially, as shown in Fig. 1(b). Specifically, $\mathbf{F}_{\mathrm{RF}}^{(i)}$, $\boldsymbol{\Phi}^{(i)}$, and $\mathbf{W}_{\mathrm{RF}}^{(i)}$ are trained through deep-unfolded MO of J inner iterations, while $\mathbf{F}_{\mathrm{BB},k}^{(i)}$ and $\mathbf{W}_{\mathrm{BB},k}^{(i)}$ are updated directly using the WMMSE algorithm. The detail is described below.

1) Updates of $\mathbf{F}_{\mathrm{RF}}^{(i)}$ With Deep-Unfolded MO: $\mathbf{F}_{\mathrm{RF}}^{(i)}$ is updated via the MO procedure [13]:

$$\mathbf{F}_{\mathrm{RF}}^{(i,j)} = f_{\mathrm{Retr}}\big(\mathbf{F}_{\mathrm{RF}}^{(i,j-1)}-\rho_{\mathrm{f}}^{(i,j)}\nabla_{\mathcal{M}}f(\mathbf{F}_{\mathrm{RF}}^{(i,j-1)})\big), \tag{11}$$

where j denotes the jth inner iteration of the MO algorithm; $\rho_{\mathrm{f}}^{(i,j)}$ is the step size; $f(\mathbf{F}_{\mathrm{RF}}^{(i,j-1)}) = [\frac{1}{K}\sum_{k=1}^{K}\mathrm{tr}(\boldsymbol{\Lambda}_k^{-1}+\beta_k^{-1}\widetilde{\mathbf{G}}_k\mathbf{F}_{\mathrm{RF}}\mathbf{F}_{\mathrm{RF}}^H\widetilde{\mathbf{G}}_k^H)^{-1}]^{(i,j-1)}$ is derived by substituting $\mathbf{F}_{\mathrm{BB},k}^{(i,j-1)}$ and $\xi_k^{(i,j-1)}$ into problem (9), with $\beta_k = \frac{\sigma^2 N_t N_r \mathrm{tr}(\boldsymbol{\Lambda}_k\mathbf{W}_{\mathrm{BB},k}^H\mathbf{W}_{\mathrm{BB},k})}{N_t^{\mathrm{RF}}N_r^{\mathrm{RF}}}$ and $\widetilde{\mathbf{G}}_k^H = \mathbf{H}_{\mathrm{eff},k}^H\mathbf{W}_k$; $\nabla_{\mathcal{M}}f(\mathbf{F}_{\mathrm{RF}}^{(i,j-1)}) = \nabla f(\mathbf{F}_{\mathrm{RF}}^{(i,j-1)}) - \mathrm{Re}\{\nabla f(\mathbf{F}_{\mathrm{RF}}^{(i,j-1)})^{(i,j-1)}\odot\mathbf{F}_{\mathrm{RF}}^{(i,j-1)}\}\odot\mathbf{F}_{\mathrm{RF}}^{(i,j-1)}$ is the Riemannian gradient calculated by projecting orthogonal components of the Euclidean gradient $\nabla f(\mathbf{F}_{\mathrm{RF}}^{(i,j-1)})$ onto the tangent space; and $f_{\mathrm{Retr}}(x) = \frac{x}{\max(0,|x|-1)+1}$ conducts element-wise retraction on $\{x|x=\mathbf{f}_m(n)\}$ to satisfy the constant modulus constraint (8c).

The MO procedure is deep unfolded through a neural network, as depicted in Fig. 1(a). Particularly, the step size $\rho_{\mathrm{f}}^{(i,j)}$ is determined by a learnable neural network followed by a normalization, i.e.,

$$\widetilde{\rho}_{\mathrm{f}}^{(i,j)} = \mathrm{LeakyReLU}\big(\mathbf{t}_{\mathrm{f}}^{(i,j)}\mathrm{V}_{\mathrm{ext}}(\mathbf{F}_{\mathrm{RF}}^{(i,j-1)})+b_{\mathrm{f}}^{(i,j)}\big), \tag{12}$$

$$\rho_{\mathrm{f}}^{(i,j)} = \frac{\widetilde{\rho}_{\mathrm{f}}^{(i,j)}}{\|\nabla_{\mathcal{M}}f(\mathbf{F}_{\mathrm{RF}}^{(i,j-1)})\|_F}. \tag{13}$$

In (12), $\mathrm{V}_{\mathrm{ext}}(\cdot)$ extracts the real and imaginary parts of the nonzero terms in $\mathbf{F}_{\mathrm{RF}}^{(i,j-1)}$ and vectorizes them, $\mathbf{t}_{\mathrm{f}}^{(i,j)} \in \mathbb{R}^{1\times 2N_t}$ and $b_{\mathrm{f}}^{(i,j)} \in \mathbb{R}$ are trainable weights and bias, respectively, and LeakyReLU denotes the activation function. In (13), a normalization based on the gradient's amplitude is performed. Compared to the step size obtained through Armijo backtracking line search, as proposed in [13], the proposed step size can accelerate the optimization process.

2) Updates of $\mathbf{F}_{\mathrm{BB},k}^{(i)}$ With WMMSE: $\mathbf{F}_{\mathrm{BB},k}^{(i)} = [\xi_k\widetilde{\mathbf{F}}_k^{-1}\mathbf{F}_{\mathrm{RF}}^H\widetilde{\mathbf{G}}_k^H\boldsymbol{\Lambda}_k]^{(i)}$, where $\xi_k = 1/\sqrt{\frac{N_t}{N_t^{\mathrm{RF}}N_s}\|\widetilde{\mathbf{F}}_k^{-1}\mathbf{F}_{\mathrm{RF}}^H\widetilde{\mathbf{G}}_k^H\boldsymbol{\Lambda}_k\|_F^2}$, $\widetilde{\mathbf{F}}_k = \mathbf{F}_{\mathrm{RF}}^H\widetilde{\mathbf{G}}_k^H\boldsymbol{\Lambda}_k\widetilde{\mathbf{G}}_k\mathbf{F}_{\mathrm{RF}} + \beta_k\mathbf{I}_{N_t^{\mathrm{RF}}}$, and $\boldsymbol{\Lambda}_k = \mathbf{E}_k^{-1}$ in the ith outer iteration.

3) Updates of $\boldsymbol{\Phi}^{(i)}$ and $\mathbf{W}_{\mathrm{RF}}^{(i)}$ With Deep-Unfolded MO: Updates of $\boldsymbol{\Phi}^{(i)}$ and $\mathbf{W}_{\mathrm{RF}}^{(i)}$ are sequentially performed in a similar manner to that of $\mathbf{F}_{\mathrm{RF}}^{(i)}$ in (11), i.e.,

$$\boldsymbol{\Phi}^{(i,j)} = f_{\mathrm{Retr}}\Big(\boldsymbol{\Phi}^{(i,j-1)}-\rho_{\Phi}^{(i,j)}\nabla_{\mathcal{M}}u\Big(\boldsymbol{\Phi}^{(i,j-1)}\Big)\Big), \tag{14}$$

$$\mathbf{W}_{\mathrm{RF}}^{(i,j)} = f_{\mathrm{Retr}}\Big(\mathbf{W}_{\mathrm{RF}}^{(i,j-1)}-\rho_{\mathrm{w}}^{(i,j)}\nabla_{\mathcal{M}}g\Big(\mathbf{W}_{\mathrm{RF}}^{(i,j-1)}\Big)\Big). \tag{15}$$

The step sizes $\rho_{\Phi}^{(i,j)}$ and $\rho_{\mathrm{w}}^{(i,j)}$ are determined using a similar neural network architecture as in (12), involving trainable parameters $\mathbf{t}_{\Phi}^{(i,j)} \in \mathbb{R}^{1\times 2M}$, $b_{\Phi}^{(i,j)} \in \mathbb{R}$ and $\mathbf{t}_{\mathrm{w}}^{(i,j)} \in \mathbb{R}^{1\times 2N_r}$, $b_{\mathrm{w}}^{(i,j)} \in \mathbb{R}$, respectively. As mentioned earlier, the weights and biases are the result of the deep unfolding technique, involving a neural network that requires training. Fig. 1 illustrates that the three MO blocks undergo individual training for their respective weights and biases during each inner and outer iteration. $g(\mathbf{W}_{\mathrm{RF}}^{(i,j-1)})$ is derived from [13]. The Euclidean gradient $\nabla g(\mathbf{W}_{\mathrm{RF}}^{(i,j-1)})$ used to calculate $\nabla_{\mathcal{M}}g(\mathbf{W}_{\mathrm{RF}}^{(i,j-1)})$ in (15) has been previously derived in [13], and its concept is similar to $\nabla_{\mathcal{M}}f(\mathbf{F}_{\mathrm{RF}}^{(i,j-1)})$. The Euclidean gradient $\nabla u(\boldsymbol{\Phi}^{(i,j-1)})$ used to calculate $\nabla_{\mathcal{M}}u(\boldsymbol{\Phi}^{(i,j-1)})$ in (14) is derived as follows. For brevity, we will omit the superscripts denoting inner and outer iterations.

We first define $u(\boldsymbol{\Phi}) = \frac{1}{K}\sum_{k=1}^{K}\mathrm{tr}(\mathbf{Q}_k^{-1})$, where $\mathbf{Q}_k = \boldsymbol{\Lambda}_k^{-1}+\beta_k^{-1}\widehat{\mathbf{G}}_k\boldsymbol{\Phi}\mathbf{C}_k\boldsymbol{\Phi}^H\widehat{\mathbf{G}}_k^H$, $\widehat{\mathbf{G}}_k = \mathbf{W}_k^H\mathbf{H}_{2,k}$, and $\mathbf{C}_k = \mathbf{H}_{1,k}\mathbf{F}_{\mathrm{RF}}\mathbf{F}_{\mathrm{RF}}^H\mathbf{H}_{1,k}^H$. It can be shown that the objective function in (9a) can be reformulated as $u(\boldsymbol{\Phi})$. Then, we derive $\nabla u(\boldsymbol{\Phi})$ by computing the gradient of $u(\boldsymbol{\Phi})$, i.e.,

$$d(u(\mathbf{\Phi})) = d\left(\frac{1}{K}\sum_{k=1}^{K}\mathrm{tr}(\mathbf{Q}_k^{-1})\right)$$
$$= -\frac{1}{K}\sum_{k=1}^{K}\mathrm{tr}\left(\mathbf{Q}_k^{-2}d(\mathbf{Q}_k)\right)$$
$$\overset{(a)}{=} -\frac{1}{K}\sum_{k=1}^{K}\mathrm{tr}\left(\beta_k^{-1}\widehat{\mathbf{G}}_k^H\mathbf{Q}_k^{-2}\widehat{\mathbf{G}}_k\mathbf{\Phi}\mathbf{C}_k d(\mathbf{\Phi}^H)\right), \quad (16)$$

where in (a), we have utilized the matrix differentiation property $d(\mathbf{XQY}) = \mathbf{X}d(\mathbf{Q})\mathbf{Y}$, with $\mathbf{X}$ and $\mathbf{Y}$ being constant matrices independent of $\mathbf{Q}$, and the trace property $\mathrm{tr}(\mathbf{AB}) = \mathrm{tr}(\mathbf{BA})$. Next, we use the properties $d(u(\mathbf{\Phi})) = \mathrm{tr}(\nabla_{\mathbf{\Phi}^*}u(\mathbf{\Phi})d(\mathbf{\Phi}^H))$ and $\nabla u(\mathbf{\Phi}) = \nabla_{\mathbf{\Phi}^*}u(\mathbf{\Phi}) \odot \mathbf{I}_M$, with the incorporation of the mask function $\mathbf{I}_M$ to comply with the diagonal matrix, where $\nabla_{\mathbf{\Phi}^*}u(\mathbf{\Phi}) = \frac{1}{K}\sum_{k=1}^{K}\beta_k^{-1}\widehat{\mathbf{G}}_k^H\mathbf{Q}_k^{-2}\widehat{\mathbf{G}}_k\mathbf{\Phi}\mathbf{C}_k$. Finally, we arrive at

$$\nabla u(\mathbf{\Phi}) = -\left(\frac{1}{K}\sum_{k=1}^{K}\beta_k^{-1}\widehat{\mathbf{G}}_k^H\mathbf{Q}_k^{-2}\widehat{\mathbf{G}}_k\mathbf{\Phi}\mathbf{C}_k\right)\odot\mathbf{I}_M. \quad (17)$$

4) Updates of $\mathbf{W}_{\mathrm{BB},k}^{(i)}$ With WMMSE: $\mathbf{W}_{\mathrm{BB},k} = (\mathbf{W}_{\mathrm{RF}}^H\mathbf{G}_k\mathbf{G}_k^H\mathbf{W}_{\mathrm{RF}} + \alpha_k\mathbf{I}_{N_r^{RF}})^{-1}\mathbf{W}_{\mathrm{RF}}^H\mathbf{G}_k$, where $\mathbf{G}_k = \xi_k^{-1}\mathbf{H}_{\mathrm{eff},k}\mathbf{F}_k$ and $\alpha_k = \frac{\sigma^2\xi_k^{-2}N_r}{N_r^{\mathrm{RF}}}$ in the ith outer iteration.

The proposed deep-unfolded WMMSE-MO algorithm employs a fixed number of inner and outer iterations. In the next outer iteration $i+1$, the update steps described above are repeated. The iterations cease when either the specified number of iterations is reached or when the relative difference between consecutive MSE values falls below a threshold [15].

The proposed deep-unfolded WMMSE-MO algorithm is trained in an unsupervised fashion, with the loss function chosen to align with the objective function defined in (8a):

$$\mathbb{L}_{\mathbf{\Theta}} = -\frac{1}{N_{\mathrm{B}}}\frac{1}{K}\sum_{n=1}^{N_{\mathrm{B}}}\sum_{k=1}^{K}R_{n,k}, \quad (18)$$

where $\mathbf{\Theta} = \{\mathbf{t}_{\mathrm{f}}^{(i,j)}, b_{\mathrm{f}}^{(i,j)}, \mathbf{t}_{\Phi}^{(i,j)}, b_{\Phi}^{(i,j)}, \mathbf{t}_{\mathrm{w}}^{(i,j)}, b_{\mathrm{w}}^{(i,j)}\}$ denotes the trainable parameters, N_{B} is the batch size, and $R_{n,k}$ represents the SE for the kth subcarrier and nth training sample in a mini-batch.

IV. Simulation Results

In this section, we present a performance comparison of the following schemes: 1) *WMMSE-MO:* the original WMMSE-MO algorithm [13] adapted for the RIS scenario, following the nested iterations framework in Fig. 1 but without deep unfolding; 2) *DU-WMMSE-MO:* the proposed deep-unfolded WMMSE-MO algorithm; 3) *T-SVD [14]:* an algorithm that optimizes the RIS by approximating mmWave channel capacity and employs a matrix factorization-based hybrid beamforming algorithm. T-SVD offers versions for both fully-connected (FC) and partially-connected (PC) structures, denoted as 'T-SVD (FC)' and 'T-SVD (PC)', respectively; 4) *T-WMMSE-MO:* an algorithm that adopts the same approach for designing RIS as in T-SVD and subsequently designs hybrid beamforming using the original WMMSE-MO algorithm; and 5) *GMD-PCA [5]:* an algorithm that designs RIS using angles of arrival and departure, plus the GMD-based baseband precoder/combiner and PCA-based analog

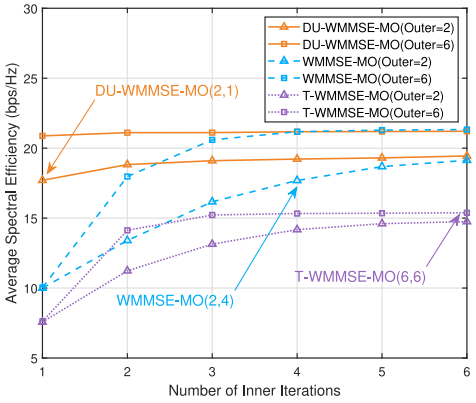

Fig. 2. Average SE vs. number of inner iterations, with SNR = 10 dB.

precoder/combiner. The system is configured with the following parameters: $N_s = 2$, $N_t = 32$, $M = 64$, $N_r = 32$, $N_t^{\mathrm{RF}} = 4$, $N_r^{\mathrm{RF}} = 4$, and $K = 16$. The channel settings include a total of $L = 51$ paths, with a Rician factor $\mu = 10$. For DU-WMMSE-MO, the dataset consists of 9000 training samples, 1000 validation samples, and 1000 testing samples. A batch size of $N_{\mathrm{B}} = 32$ is used, and the Adam optimizer is employed with a learning rate of 0.001. The training process concludes after 30 epochs.

First, we examine the convergence speed of WMMSE-MO-based algorithms, as shown in Fig. 2. The notation (*I, J*) represents I outer iterations and J inner iterations. As can be seen, DU-WMMSE-MO exhibits accelerated convergence and achieves substantial performance improvements in the initial stages of iteration. Notably, DU-WMMSE-MO(2,1) outperforms WMMSE-MO(2,4) and T-WMMSE-MO(6,6), highlighting the superior performance of DU-WMMSE-MO with fewer inner and outer iterations. DU-WMMSE-MO consistently outperforms T-WMMSE-MO in all configurations. All the schemes reach saturation as the number of inner iterations increases. The advantages of the proposed DU-WMMSE-MO can be attributed to two main factors. First, DU-WMMSE-MO designs the RIS as part of the sequence in each outer iteration, as depicted in Fig. 1(b). In contrast, T-WMMSE-MO first completes the RIS design and then performs the hybrid beamforming design based on the constructed RIS and the resultant effective channel. The approach adopted in DU-WMMSE-MO contributes to the enhanced RIS phase shift design. Second, DU-WMMSE-MO adopts a training-based step size update process, which offers more flexibility compared to the Armijo backtracking line search method used by T-WMMSE-MO and WMMSE-MO. This enhanced flexibility contributes to faster convergence and superior performance of DU-WMMSE-MO.

Next, we compare the performance of all schemes across various signal-to-noise ratio (SNR) values. Figs. 3(a) and 3(b) show the results for 1 and 4 inner iterations, respectively, for WMMSE-MO-based schemes. All schemes operate under the partially-connected structure except T-SVD (FC). In Fig. 3(a), the proposed DU-WMMSE-MO is superior over T-WMMSE-MO and WMMSE-MO as previously mentioned. Additionally, with an increase in the number of outer iterations from 2 to 6, DU-WMMSE-MO exhibits enhanced performance, achieving an average SE improvement from 17.7 to 20.9 bps/Hz at SNR = 10 dB. In contrast, both T-WMMSE-MO and WMMSE-MO do not achieve comparable advancements

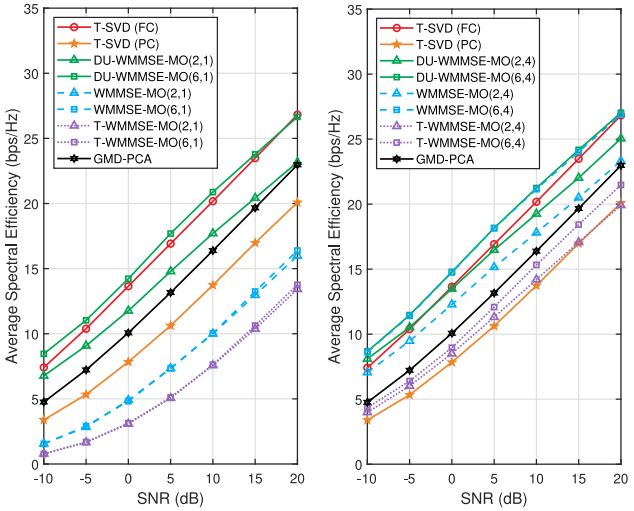

Fig. 3. Average SE vs. SNR, with (a) 1 and (b) 4 inner iterations for WMMSE-MO-based schemes.

TABLE I
AVERAGE RUNTIME (UNIT: SECOND)

Scheme	(2, 1)	(2, 4)	(6, 1)	(6, 4)
DU-WMMSE-MO	0.0162	0.0339	0.0438	0.0961
WMMSE-MO	0.0205	0.0521	0.0474	0.2565
T-WMMSE-MO	0.0082	0.0190	0.0166	0.0499
T-SVD (FC)	0.042			
T-SVD (PC)	0.0316			
GMD-PCA	0.0109			

in performance. The training-based step size adopted in DU-WMMSE-MO contributes to the improvement. Moreover, the proposed DU-WMMSE-MO(2,1) outperforms T-SVD (PC) and GMD-PCA, since the proposed DU-WMMSE-MO iteratively updates beamforming and RIS matrices to achieve a better joint design, while others first optimize RIS and then beamforming matrices, which could result in performance degradation. Moreover, as the number of outer iterations reaches 6, DU-WMMSE-MO(6,1) exceeds the performance of T-SVD (FC). This shows that the proposed method can achieve superior performance with simplified hardware connections and reduced hardware costs. Comparing Figs. 3(a) and 3(b), the average SE improves as the number of inner iterations increases for DU-WMMSE-MO, WMMSE-MO, and T-WMMSE-MO.

Finally, we compare the average runtime for all schemes in Table I. T-WMMSE-MO exhibits relatively lower runtime compared to DU-WMMSE-MO and WMMSE-MO due to its one-pass RIS design, in contrast to the multiple outer iterations involved in the other two schemes. However, this reduction in runtime comes at the cost of significantly worse SE performance. To assess the extent of acceleration achieved by the deep unfolding technique, we observe that DU-WMMSE-MO(2,4) achieves a substantial runtime reduction of 34.93% compared to the WMMSE-MO counterpart, approaching the computation time of T-SVD (PC) even though DU-WMMSE-MO(2,4) significantly outperforms T-SVD (PC) in SE performance. Furthermore, DU-WMMSE-MO(2,1) and GMD-PCA have comparable complexity; however, the achieved average SE of the former is 1.3 bps/Hz higher than the latter at SNR $=$ 10 dB. The complexity reduction of DU-WMMSE-MO compared to WMMSE-MO is even more pronounced for the (6,4) setting, reaching 62.53%. Overall, the results demonstrate the effectiveness of the proposed deep unfolding approach and the favorable balance between performance and complexity achieved by the DU-WMMSE-MO scheme.

V. CONCLUSION

In this letter, we have applied the WMMSE-MO algorithm to the joint hybrid beamforming and RIS design problem in RIS-aided mmWave MIMO-OFDM systems. We incorporated the deep unfolding technique to optimize the iterative algorithm's step size, leading to improved convergence speed, performance, and computational efficiency. Our proposed DU-WMMSE-MO scheme, which employs a partially-connected structure, carries the potential to outperform T-SVD (FC) utilizing a fully-connected structure, highlighting the cost-effectiveness of our method.

REFERENCES

[1] I. Ahmed et al., "A survey on hybrid beamforming techniques in 5G: Architecture and system model perspectives," *IEEE Commun. Surveys Tuts.*, vol. 20, no. 4, pp. 3060–3097, 4th Quart, 2018.
[2] Q. Wu, S. Zhang, B. Zheng, C. You, and R. Zhang, "Intelligent reflecting surface-aided wireless communications: A tutorial," *IEEE Trans. Commun.*, vol. 69, no. 5, pp. 3313–3351, May 2021.
[3] Q. Wu and R. Zhang, "Towards smart and reconfigurable environment: Intelligent reflecting surface aided wireless network," *IEEE Commun. Mag.*, vol. 58, no. 1, pp. 106–112, Jan. 2020.
[4] S. H. Hong, J. Park, S.-J. Kim, and J. Choi, "Hybrid beamforming for intelligent reflecting surface aided millimeter wave MIMO systems," *IEEE Trans. Wireless Commun.*, vol. 21, no. 9, pp. 7343–7357, Sep. 2022.
[5] K. Ying, Z. Gao, S. Lyu, Y. Wu, H. Wang, and M.-S. Alouini, "GMD-based hybrid beamforming for large reconfigurable intelligent surface assisted millimeter-wave massive MIMO," *IEEE Access*, vol. 8, pp. 19530–19539, 2020.
[6] K. Feng, X. Li, Y. Han, and Y. Chen, "Joint beamforming optimization for reconfigurable intelligent surface-enabled MISO-OFDM systems," *China Commun.*, vol. 18, no. 3, pp. 63–79, Mar. 2021.
[7] B. Sheen, J. Yang, X. Feng, and M. M. U. Chowdhury, "A deep learning based modeling of reconfigurable intelligent surface assisted wireless communications for phase shift configuration," *IEEE Open J. Commun. Soc.*, vol. 2, pp. 262–272, 2021.
[8] J. Gao, C. Zhong, X. Chen, H. Lin, and Z. Zhang, "Unsupervised learning for passive beamforming," *IEEE Commun. Lett.*, vol. 24, no. 5, pp. 1052–1056, May 2020.
[9] H. Song, M. Zhang, J. Gao, and C. Zhong, "Unsupervised learning-based joint active and passive beamforming design for reconfigurable intelligent surfaces aided wireless networks," *IEEE Commun. Lett.*, vol. 25, no. 3, pp. 892–896, Mar. 2021.
[10] A. Jagannath, J. Jagannath, and T. Melodia, "Redefining wireless communication for 6G: Signal processing meets deep learning with deep unfolding," *IEEE Trans. Artif. Intell.*, vol. 2, no. 6, pp. 528–536, Dec. 2021.
[11] Y. Liu, Q. Hu, Y. Cai, G. Yu, and G. Y. Li, "Deep-unfolding beamforming for intelligent reflecting surface assisted full-duplex systems," *IEEE Trans. Wireless Commun.*, vol. 21, no. 7, pp. 4784–4800, Jul. 2022.
[12] J. He, H. Wymeersch, M. Di Renzo, and M. Juntti, "Learning to estimate RIS-aided mmWave channels," *IEEE Wireless Commun. Lett.*, vol. 11, no. 4, pp. 841–845, Apr. 2022.
[13] X. Zhao, T. Lin, Y. Zhu, and J. Zhang, "Partially-connected hybrid beamforming for spectral efficiency maximization via a weighted MMSE equivalence," *IEEE Trans. Wireless Commun.*, vol. 20, no. 12, pp. 8218–8232, Dec. 2021.
[14] P. Wang, J. Fang, L. Dai, and H. Li, "Joint transceiver and large intelligent surface design for massive MIMO mmWave systems," *IEEE Trans. Wireless Commun.*, vol. 20, no. 2, pp. 1052–1064, Feb. 2021.
[15] T. Lin, J. Cong, Y. Zhu, J. Zhang, and K. B. Letaief, "Hybrid beamforming for millimeter wave systems using the MMSE criterion," *IEEE Trans. Commun.*, vol. 67, no. 5, pp. 3693–3708, May 2019.